https://doi.org/10.5194/bg-2022-238
Preprint. Discussion started: 13 February 2023

Biogeosciences Discussions Open Access EGU

Enabling a process-oriented hydro-biogeochemical model to simulate soil erosion and nutrient losses

Siqi Li [a, b], Bo Zhu [c], Xunhua Zheng [a, d], Pengcheng Hu [c], Shenghui Han [a], Jihui Fan [c], Tao Wang [c], Rui Wang [a], Kai Wang [a], Zhisheng Yao [a], Chunyan Liu [a], Wei Zhang [a, *], Yong Li [a, *]

[a] State Key Laboratory of Atmospheric Boundary Layer Physics and Atmospheric Chemistry, Institute of Atmospheric Physics, Chinese Academy of Sciences, Beijing 100029, China

[b] State Environmental Protection Key Laboratory of Formation and Prevention of Urban Air Pollution Complex, Shanghai Academy of Environment Sciences, Shanghai 200233, P. R. China

[c] Institute of Mountain Hazards and Environment, Chinese Academy of Sciences, Chengdu 610041, China

[d] College of Earth and Planetary Science, University of Chinese Academy of Sciences, Beijing 100049, China

[*] Corresponding author

Tel.: +86 10 13681042146

+86 10 13107488562

E-mail address: zhangwei87@mail.iap.ac.cn (W. Zhang)

yli@mail.iap.ac.cn (Y. Li)

https://doi.org/10.5194/bg-2022-238
Preprint. Discussion started: 13 February 2023


Biogeosciences Discussions Open Access EGU

Abstract

Water-induced erosion and subsequent particulate carbon (C), nitrogen (N) and phosphorus (P) nutrient losses were the vital parts of biogeochemical cycling. Identifying their intensity and distribution characteristics is of great significance for the control of soil and water loss and N/P nonpoint source pollution. This study incorporated the modules of physical soil erosion and the particulate C, N and P losses into the process-oriented hydro-biogeochemical model (CNMM-DNDC) to enable it to predict soil and water loss. The results indicated that the upgraded CNMM-DNDC i) performed well in simulating the observed temporal dynamics and magnitudes of surface runoff, sediment and particulate N/P losses in the lysimetric plot of the Jieliu catchment in Sichuan Province; ii) successfully predicted the observed monthly dynamics and magnitudes of stream flow, sediment yield and particulate N losses at the catchment outlet, with significant zero-intercept univariate linear regressions and credible Nash–Sutcliffe indices larger than 0.74. The particulate N accounted for 16.2%−26.6% of the TN components during the period with larger precipitations. The intensities of soil erosion and particulate nutrient losses in the Jieliu catchment was closely related to land use type in the order of sloping cultivated cropland > residential area > forest land. The scenario analysis demonstrated that high greenhouse gas (GHG) emissions scenarios provided a greater risk of soil erosion than did low GHG emissions scenarios and land use change could help to mitigate soil and water loss accelerated by climate change in the future. The upgraded model was demonstrated to have the capability of predicting ecosystem productivity, hydrologic nitrogen loads, emissions of GHGs and pollutant gases, soil erosion and particulate nutrient losses, which may become a decision

https://doi.org/10.5194/bg-2022-238
Preprint. Discussion started: 13 February 2023

support tool for soil erosion and nonpoint source pollution control coordinated with increasing production and reducing GHGs and pollutant gases emissions in a catchment.

Keywords

CNMM-DNDC, ROSE, soil erosion, particulate carbon/nitrogen/phosphorus loss

1. Introduction

Water-induced erosion and subsequent particulate carbon (C), nitrogen (N) and phosphorus (P) nutrient losses are among the primary threats leading to the decline in soil fertility and the increases in land degradation, channel sedimentation and eutrophication of downstream rivers and lakes (Berhe et al., 2018; Ekholm and Lehtoranta, 2012; Garcia-Ruiz et al., 2015). This global environmental issue has continued to deteriorate (Ma et al., 2021; Yang et al., 2003). A previous study found that the vulnerability of water-induced erosion increased over 51% of the global surface from 1982 to 2015 (Liu et al., 2019). Climate change and anthropogenic activities (such as land use change) are the two principal driving forces that have complicated and altered the hydrological cycle and water-induced erosion during recent decades (Piao et al., 2007; Zeng et al., 2015).

Quantitative assessments of the water-induced soil erosion intensity and identification of its temporal and spatial distribution characteristics are of great importance for preventing soil and water loss and have attracted the attention of researchers (e.g., Jetten et al., 2003; Jiang et al., 2017; Panagos et al., 2015). Lysimetric plot experiments have been developed as a direct field measurement method for the accurate quantification of surface runoff and water-induced erosion (e.g., Kosmas et al., 1997; Sumner et al., 1996; Zhu et al., 2009). However, the in situ field measurements of water-reduced soil erosion with high cost of labor and money can only

https://doi.org/10.5194/bg-2022-238
Preprint. Discussion started: 13 February 2023

63 cover a small piece of the sampling units. It is unrealistic to expect direct field measurements
64 to quantify water-induced erosion everywhere under various conditions.

65 Simulations of mathematical models are likely to compensate for the deficiency of direct
66 field measurements. The Universal Soil Loss Equation (USLE, Wischmeier and Smith, 1978)
67 and its revised version (RUSLE) (Renard et al., 1997) have been developed into widely used
68 empirical mathematical models to directly calculate soil erosion based on rainfall, soil property,
69 topography, cover and management data. The USLE or RUSLE quantify only the various
70 influencing factors that impact the soil loss associated with soil erosion, which is not directly
71 related to the process of surface runoff and does not involve the specific process of sediment
72 transport yet (Donovan, 2022; Meinen and Robinson, 2021). Fortunately, the physical
73 process-based ROSE model named after the name of developer (Rose et al., 1983)
74 conceptualizes the soil erosion process by conceiving three continuous and simultaneous
75 physical processes, including rainfall detachment, sediment entrainment and sediment
76 deposition, thus providing good performance in estimating sediment yield at the plot scale.
77 However, the ROSE model focuses only on the physical processes of water-induced erosion
78 without engaging the C and N cycles of the ecosystem. The Soil and Water Assessment Tool
79 (SWAT) (Arnold et al., 1998), a semi distributed hydrological model, incorporates the RUSLE
80 to predict soil erosion at the level of hydrological response units, in which the routing of
81 sediment transportation is not considered and the modeling of the biogeochemical element
82 cycle is relatively simple and empirical (Ferrant et al., 2011; Pohlert et al., 2007). However, the
83 transport of particulate C, N, and P nutrients accompanied by water-induced erosion crucially

https://doi.org/10.5194/bg-2022-238
Preprint. Discussion started: 13 February 2023

84 depends on the C and N cycles of ecosystems in a catchment. Therefore, knowledge of the
85 coupling between the process-oriented hydro-biogeochemical model combined with the
86 complicated C and N cycles and the soil erosion model based on physical processes (such as
87 ROSE) is essential to accurately predict soil erosion and subsequent particulate C, N, and P
88 nutrient transport.

89 A recently developed hydro-biogeochemical model (CNMM-DNDC) by Zhang et al.
90 (2018) might become a realistic tool that can be used to address the abovementioned problem.
91 The CNMM-DNDC model introduces the complicated C and N biogeochemical modules
92 (including the modules of decomposition, nitrification, denitrification and fermentation) of a
93 widely used biogeochemical model (DeNitrification-DeComposition model, DNDC, Li et al.,
94 1992) into the distributed hydrological framework of the Catchment Nutrients Management
95 Model (CNMM, Li et al., 2017). The CNMM-DNDC model has been used to conduct a
96 comprehensive simulation of the complicated hydrological and biogeochemical processes
97 (such as ecosystem productivity, hydrologic N loads, gaseous N losses and greenhouse gas
98 emissions) of a subtropical catchment with various landscapes (Zhang et al., 2018), a model
99 evaluation of nitrous oxide and nitric oxide emissions from a subtropical tea plantation (Zhang
100 et al., 2020b), a model evaluation and regional simulation of nitrate leaching in the black soil
101 region of Northeast China (Zhang et al., 2021a) and a comprehensive model modification and
102 evaluation of NH_3 volatilization from fertilized croplands (Li et al., 2022b). However, the
103 CNMM-DNDC model still lacks the capacity to simulate the processes of soil erosion and
104 subsequent particulate C, N, and P nutrient transportation.

https://doi.org/10.5194/bg-2022-238
Preprint. Discussion started: 13 February 2023

Therefore, we hypothesize that the accurate simulation of soil erosion and subsequent particulate C, N, and P nutrient losses can be realized by incorporating the soil erosion physical model and the element enrichment module into the process-oriented hydro-biogeochemical model with complicated C and N cycles. Based upon the above hypothesis, the objectives of this study were to i) introduce the ROSE model (a physical soil erosion model) and the enrichment module of the particulate nutrients into the hydrological process of the CNMM-DNDC model; ii) evaluate the performance of the CNMM-DNDC model in simulating the temporal and spatial distributions of soil erosion and subsequent particulate C, N, and P transportation at the plot and catchment scales; and iii) investigate the impact of climate change and human activities (such as land use change) on the losses of soil and particulate nutrients.

2. Materials and methods

2.1 Catchment description

The Jieliu catchment (31°16′N, 105°28′E, 400−600 m a.s.l.), located in Sichuan Province of Southwest China (Zhu et al., 2009), was used for the model calibration and validation. This catchment is situated in the upper reaches of the Yangtze River and has a typical subtropical monsoon climate. During the period from 2005 to 2018, the annual mean temperature was 16.7 ℃, and the average annual precipitation was 720 mm, 75% of which occurred during the period between June and September (http://yga.cern.ac.cn). The soil in the catchment is dominated by Calcaric purple soil, classified as a Pup-Orthic Entisol in the Chinese Soil Taxonomy or as an Entisol classified in the U.S. Soil Taxonomy (Zhu et al., 2009). The total area of the Jieliu catchment is approximately 35 ha, and it is dominated by sloping croplands (54%) and forest lands (31%). The primary crops cultivated in the sloping croplands are maize

https://doi.org/10.5194/bg-2022-238
Preprint. Discussion started: 13 February 2023

(Zea mays L.), winter wheat (Triticum aestivum L.), rape (Brassica napus L.) and rice (Oryza sativa L.). The N, P and potassium (K) fertilizers are applied at rates of 130–330 kg N ha^{-1} yr^{-1} (ammonium bicarbonate or urea), 72–162 kg P ha^{-1} yr^{-1} (calcium superphosphate) and 45–68 kg K ha^{-1} yr^{-1} (potassium chloride), respectively (Zhang et al., 2018).

2.2 Model modifications

The CNMM-DNDC model can simulate the lateral movements of water-soluble nutrients (e.g., ammonium, nitrate, phosphate and dissolved organic matter) by surface and subsurface runoff, whereas it lacks the capabilities of simulating soil erosion and sediment transport caused by surface runoff and the subsequent transportation of particulate C, N, and P. To address such a deficiency, this study incorporated the modules of soil erosion and element enrichment into the lateral hydrological framework of the CNMM-DNDC model. Therefore, the upgraded CNMM-DNDC model was equipped with the ability to estimate the movements of soil particles and particulate nutrients transported with surface runoff in the lateral dimension. The soil erosion module adopted the simplified ROSE model (Rose et al., 1983; Stewart, 1985), which is a process-oriented soil erosion model. The ROSE model is based on the dynamic equilibrium of three simultaneous processes, including rainfall detachment, runoff detachment, and sediment deposition. In an individual erosion event, the process of runoff detachment dominates, and the latter two processes of rainfall detachment and sediment deposition can be generally neglected. Therefore, in the simplified ROSE module, as shown by Eq. (1), the sediment yield (Y_s, kg dry soil ha^{-1}) resulting from soil erosion was driven by surface runoff (R_s, m) and concomitantly regulated by the land's slope (S_l, dimensionless) and

https://doi.org/10.5194/bg-2022-238
Preprint. Discussion started: 13 February 2023

148 the coverage fraction of vegetation (C_v, fraction).

$$Y_s = 27 \times 10^6 (1 - C_v) \eta S_l R_s \quad (1)$$

149 Where R_s is calculated from the existing hydrological module of the CNMM-DNDC
150 model, in which R_s occurs in the following two cases. First, R_s is caused by the mechanism of
151 excess infiltration, in which the water input (i.e., precipitation and irrigation) is greater than the
152 maximum infiltration capacity of the soil. Second, R_s is derived from the mechanism of excess
153 storage, in which precipitation or irrigation still occurs when the soil surface water content
154 exceeds the corresponding saturated water content. The direction of the surface runoff conflux
155 is estimated by the distributed weights of four neighboring grids (i.e., in the upper, lower, left
156 and right directions), which are calculated based on the elevation of these grids. S_l is the sine
157 value of the slope radian value. In this study, the value of C_v for the crop is approximately
158 equivalent to the growing index, which is estimated by the ratio of the accumulated
159 temperature from sowing to the present time to the accumulated thermal degree for maturity in
160 the plant growth module. Particularly, using the observed sediment yield in the catchment
161 outlet, the value of C_v for the natural vegetation (e.g., forest and grass) was addressed and
162 calibrated as half of the ratio of the real leaf area index (LAI) and the maximum LAI, which is
163 one of the model inputs. The value of C_v of the artificial lands (e.g., the urban or rural
164 residential areas) was calibrated and set to 0.1, which represented the effects of concrete roads
165 and residential buildings on the reduction of the soil area exposed to erosion. Usually, the
166 values of C_v need to be calibrated by the soil exposure ratio and sediment yield observations

https://doi.org/10.5194/bg-2022-238
Preprint. Discussion started: 13 February 2023


Biogeosciences Discussions Open Access EGU

for a given study area. η (dimensionless) is referred to as the efficiency of sediment entrained by surface runoff, which depends on soil texture and C_v, as shown in Eq. (2). In Eq. (2), a_1 is referred to as the rate of sediment carried by surface runoff on bare land, which differs for various soil types and generally needs to be calibrated by the observed data of sediment loss for a given study area. Loch and Donnollan (1983) reported that a_1 varies from 1.0% to 8.7% in Middle Ridge clay loam and Irving clay soils. The soil mass balance was not considered in the upgraded model.

$$\eta = a_1 e^{-0.15 C_v} \quad (2)$$

It is known that the C, N, and P elements of the eroded sediments are usually richer than those of the in situ soils from which the eroded sediments originate (Massey and Jackson, 1952; Schiettecatte et al., 2008; Wan and El-Swaify, 1998). The above phenomenon is usually referred to as sediment enrichment, which can be quantified by an empirically based enrichment ratio (E). E is usually defined as the ratio of the concentration of C, N, and P elements in the eroded sediment to that in the source soil (Sharpley, 1980; Teixeira and Misra, 2005). Generally, as more eroded sediment is produced, the richness of the C, N, and P elements decreases. The enrichment ratio of the C and N nutrients (E_{CN}) is estimated by Eq. (3), which was adapted from McElroy et al. (1976) and Williams and Hann (1978). The pre-exponential factor (k_1) of Eq. (3) was calibrated to 1.2 using the particulate N data observed at the lysimetric plot in this study. The enrichment ratio of P nutrients (E_P) is calculated by Eq. (4) cited from Sharpley (1980).

https://doi.org/10.5194/bg-2022-238
Preprint. Discussion started: 13 February 2023

$$E_{\mathrm{CN}} = k_1(Y_{\mathrm{s}} \times 10^{-4})^{-0.2468} \quad (3)$$

$$E_{\mathrm{P}} = e^{(2.46-0.2\log Y_{\mathrm{s}})} \quad (4)$$

186 The yields of particulate C (P_{C}, kg C ha^{-1}), N (P_{N}, kg N ha^{-1}), and P (P_{P}, kg P ha^{-1})
187 nutrients caused by soil erosion were calculated based on E, Y_{s} and the content of the
188 corresponding organic C (C_{C}, g C ha^{-1}), N (C_{N}, g N ha^{-1}), and P (C_{P}, g P ha^{-1}) pools in topsoil
189 using Eqs. (5–7), respectively. BD (g m^{-3}) and D_{s} (m) refer to the soil bulk density and the
190 depth of topsoil, respectively. Eight of the soil organic C and N subpools participated in the
191 process of soil erosion, including the pools of very reliable, reliable, and resistant
192 decomposable litters, reliable and resistant active microbes, reliable and resistant humads and
193 passive humus, whereas five of the soil organic P subpools were involved in the process of soil
194 erosion, including the pools of active and passive organic P, active and dead microorganism P,
195 and inert stable P. The particulate C, N, and P losses calculated by the element enrichment
196 module were also deducted from the corresponding subpools of the topsoil. Subsequently, the
197 eroded soil and the particulate C, N, and P nutrients are transported with surface runoff and
198 eventually drain into streams.

$$P_{\mathrm{C}} = \sum_{i=1}^{8} \frac{10^{-7} E_{\mathrm{CN}} C_{\mathrm{C}_i} Y_{\mathrm{s}}}{\mathrm{BD} \cdot D_{\mathrm{s}}} \quad (5)$$

$$P_{\mathrm{N}} = \sum_{j=1}^{8} \frac{10^{-7} E_{\mathrm{CN}} C_{\mathrm{N}_j} Y_{\mathrm{s}}}{\mathrm{BD} \cdot D_{\mathrm{s}}} \quad (6)$$

https://doi.org/10.5194/bg-2022-238
Preprint. Discussion started: 13 February 2023

$$P_{\mathrm{P}} = \sum_{k=1}^{5} \frac{10^{-7} E_{\mathrm{P}} C_{\mathrm{P}_k} Y_{\mathrm{s}}}{\mathrm{BD} \cdot D_{\mathrm{s}}} \quad (7)$$

199 **2.3 Preparation for model simulation**

200 The input data for driving the model operation consisted of the meteorological data at the
201 3-hour scale (including average air temperature, solar radiation, long wave radiation, wind
202 speed, humidity and total precipitation), the spatialized soil properties (including soil texture,
203 soil organic carbon, bulk density and pH), the gridded digital elevation model (DEM, Fig. 1)
204 with a resolution of 5 m × 5 m, the spatial distribution of land use (Fig. 1) and cropping systems,
205 and the field management practices. Taking the efficiency of the model calculation and the
206 accuracy of the biogeochemical process description into consideration, the upgraded
207 CNMM-DNDC model conducted a simulation with a grid of 15 m × 15 m from 2004 to 2017,
208 with an initial spin-up period of ten years. The DEM, soil properties, land use, cropping
209 systems, field management practices and meteorological data from 2004 to 2014 were
210 primarily adapted from Zhang et al. (2018). The remaining meteorological data were adapted
211 from the hourly observations provided at the National Science & Technology Infrastructure
212 (http://rs.cern.ac.cn). The input data of soil properties, DEM, land use, cropping systems, and
213 field management practices were resampled to the ASCII grids with a resolution of 15 m × 15
214 m using the ArcGIS 10.0 software package (ESRI, Redland, CA, USA). The observation data
215 measured at the lysimetric plot and the catchment outlet (Fig. 1) contributed to model
216 calibration and validation. The surface runoff, subsequent sediment yield, and particulate and
217 total N losses from 2004 to 2006 with three replicates and the surface runoff, subsequent
218 sediment yield, and total P loss from 2017 to 2018 with three replicates measured at the

https://doi.org/10.5194/bg-2022-238
Preprint. Discussion started: 13 February 2023

lysimetric plots were adapted from Deng et al. (2011) and Hu (2020), respectively. The monthly stream flow, sediment yield, and particulate and total N losses from 2007 to 2008 measured at the catchment outlet were directly cited from Deng et al. (2011). Total N referred to the total amount of NH_4^+, NO_3^-, dissolved organic N and particulate N. Total P referred to the total amount of dissolved organic and inorganic P and particulate P. Among them, the observed data from the lysimetric plot in 2004 (with seven observation times) and 2016 (with four observation times and a heavy precipitation event) and the observed data from the catchment outlet in 2007 were used for model calibration, and the remaining observed data were used for model validation.

2.4 Climate and land use scenario settings

Scenario analysis was adopted to assess the impact of climate change and land use change on water-induced erosion and its accompanying nutrient losses. The annual accumulated yields of sediment and particulate C, N, and P nutrient losses at the outlet in 2008 (the year for model validation) simulated by the upgraded model were used as the baseline values of the scenario analysis. Two groups of climate change and land use change scenarios were designed: single-factor change and multifactor change scenarios. The single-factor change scenarios altered only one factor while keeping the others constant. The single-factor change scenarios of climate change consisted of two parts. One part for air temperature change was altered within the range of −4 ℃ to +4 ℃ with an interval of 0.2 ℃ (abbreviated as T_{air}+ the increase value of air temperature or T_{air}− the decrease value of air temperature). The other part for precipitation change was altered by the range from −30% to +30% with an interval of 2%

https://doi.org/10.5194/bg-2022-238
Preprint. Discussion started: 13 February 2023

240 (abbreviated as *P*+ the increase percentage of precipitation or *P*− the decrease percentage of
241 precipitation). A single-factor change scenario of land use was designed as the sloping upland
242 changed into forest land with the lower soil erosion rate (i.e., FL scenario). The existing land
243 use conversion to another type, such as the change from cropland to forest land or some other
244 land use, is a kind of compromise and required a sensitivity analysis to the model simulation
245 rather than representing the conditions of the real natural system (Dey and Mishra, 2017). The
246 multifactor change group was designed to simultaneously consider climate and land use change.
247 The IPCC's Summary for Policy-makers (IPCC, 2021) points out that the average annual
248 global land precipitation is projected to increase by 10.5% and 30.2% at the 1.5 ℃ and 4 ℃
249 warming levels, respectively. According to the correspondence between climate warming and
250 increasing precipitation in the IPCC's AR6, the multifactor change scenarios designed two
251 multiple climate change scenarios: the low and high greenhouse gas (GHG) emissions
252 scenarios. The low GHG emissions scenario represents air temperature and precipitation
253 increasing by 1.5 ℃ and 10%, respectively, while the high one represents air temperature and
254 precipitation increasing by 4 ℃ and 30%, respectively. For the sake of argument, we also
255 divided air temperature and precipitation single-factor scenarios into four sets. The scenarios
256 with air temperature increases greater than 2 ℃ were defined as the higher warming scenarios,
257 while the lower ones were defined as the scenarios with air temperature changes from 0 ℃ to
258 2 ℃. The scenarios with air temperature reductions greater than 2 ℃ were defined as the
259 higher cooling scenarios, while the lower cooling scenarios were defined as the scenarios with
260 air temperature changes from −2 ℃ to 0 ℃. Similarly, the scenarios with precipitation

https://doi.org/10.5194/bg-2022-238
Preprint. Discussion started: 13 February 2023

increases greater than 20% were defined as the higher rain-enhanced scenarios, while the lower ones were defined as the scenarios with precipitation changes from 0% to 20%. The scenarios with precipitation decreasing more than 20% were defined as the higher rain-reduced scenarios, while the lower rain-reduced scenarios were defined as the scenarios with precipitation change from −20% to 0%. Furthermore, we also explored the effect of the low and high GHG emissions scenarios in a combination of land use change scenarios (i.e., FL scenario) on sediment yield and particulate nutrient yields. The tillage scenario analysis was involved in the scenario analysis of alternative management practices, which were conducted as the no tillage operations of the short term in 2008 and the long term from 2004 to 2008. The relative change deviations of the simulated annual accumulated sediment and particulate nutrient losses of the designed scenarios from the baseline were provided as the quantitative evaluation index for scenario analysis (Abdalla et al., 2020; Dubache et al., 2019).

2.5 Evaluation of model performance and statistical analysis

The performance of the upgraded CNMM-DNDC model in simulating sediment and particulate nutrient losses was evaluated using the normalized root mean square error (nRMSE), the Nash–Sutcliffe index (NSI) and the slope, determination coefficient (R^2) and significance level (p) of the zero-intercept univariate linear regression (ZIR) between the simulation and observation. The nRMSE and NSI values are calculated by Eq. 8 and Eq. 9, respectively. O_i and S_i are the observed and simulated values, respectively. $\overline{O}$ is the mean value of the observed data, and n is the number of paired samples. If the value of nRMSE is closer to 1, the values simulated by the model are more coincident with the observed values (Cui et al., 2014;

https://doi.org/10.5194/bg-2022-238
Preprint. Discussion started: 13 February 2023

Smith et al., 1997). The value of the NSI provides the discrepancy between the simulated values and the mean of the observed values, with a positive value indicating an acceptable simulation (Li et al., 2022a). The closer to 1 the slope and R^2 of the ZIR are, the better the simulated values match the observed values. The Origin 8.0 (OriginLab Ltd., Guangzhou, China) and ArcGIS 10.0 software packages were used for graph drawing.

$$\mathrm{nRMSE} = \frac{100}{\overline{O}}\sqrt{\frac{\sum_{i=1}^{n}(S_i - O_i)^2}{n}} \tag{8}$$

$$\mathrm{NSI} = 1 - \frac{\sum_{i=1}^{n}(S_i - O_i)^2}{\sum_{i=1}^{n}\left(O_i - \overline{O}\right)^2} \tag{9}$$

In addition, linear correlations were carried out to study the relationships between the variables relevant to soil erosion and that related to the biogeochemistry process. The R project was applied for the graph drawing of correlation matrix.

3. Results

3.1 Model performance in simulating soil erosion in the lysimetric plot

Among the only eight soil erosion observations conducted at the lysimetric plot from 2015 to 2017, four observations in 2016 were provided for model calibration. Given the limited size of the samples, the performance of the upgraded CNMM-DNDC model was revealed using only the graph of the predictions and observations (Fig. 2a−c), without a quantitative evaluation with the above statistical criteria. The temporal dynamic patterns of the simulated surface runoff, sediment and concomitant particulate P yields were in accordance with the observed values when either model calibration or validation was performed (Fig. 2 a−c). Nevertheless, on July 23, which was a heavy precipitation event (213 mm precipitation during

https://doi.org/10.5194/bg-2022-238
Preprint. Discussion started: 13 February 2023

the seven days prior to the observation day) in 2016, the upgraded model overestimated the observed sediment yield by approximately 6 times (3.6 versus 0.6 t ha^{-1}, Fig. 2b). However, the simulated surface runoff and total P loss were only approximately 60% and 20% larger than the observed values, respectively. Unfortunately, the simulated peaks of surface runoff and sediment yield at the end of June 2015 lacked the support of the observations. Previous results by the authors also demonstrated that the upgraded CNMM-DNDC performed well in simulating surface runoff, sediment yield, and particulate N loss in 2004 (i.e., the verification period) in the lysimetric plot, with significant ZIRs and credible nRMSE values of 15.2%, 32.0%, and 88.0%, respectively (Table S1 and Fig. 2d−g). Moreover, we conducted an evaluation of the simulated and observed NH_4^+ and NO_3^- losses accompanied by surface runoff in the lysimetric plot (Fig. S1). The upgraded model generally captured the temporal variation and magnitude of the observed NH_4^+ and NO_3^- loss, although discrepancies existed in the magnitude of the peak loss (i.e., the model underestimated NH_4^+ loss caused by approximately 100 mm precipitation on September 4, 2006; Fig. S1).

3.2 Model performance in simulating soil erosion at the catchment outlet

The monthly observed and simulated stream flow, sediment yield, particulate and total N losses at the outlet of the Jieliu catchment from 2007 to 2008 are illustrated in Fig. 3. The observed stream flow and sediment yield began to increase dramatically with the concentrated precipitation in summer and early autumn but rarely occurred in winter and spring (Fig. 3a−c). The upgraded CNMM-DNDC model successfully predicted the above temporal pattern of the stream flow and sediment yield at the catchment outlet with credible NSI values of 0.89 and

https://doi.org/10.5194/bg-2022-238
Preprint. Discussion started: 13 February 2023

321 0.89 and significant ZIRs with R^2 values of 0.94 and 0.92 and slope values of 0.85 and 0.88 for
322 model validation, respectively (Table 1). Moreover, model validation of sediment yield resulted
323 in a larger nRMSE (38.23%) than that of stream flow simulation (34.57%).

324 The observed particulate and total N losses revealed a similar temporal pattern to that of
325 sediment yield (Fig. 3d−e) ranged from 0 to 56.3 kg mon^{-1} and 0.9 to 283.1 kg N mon^{-1} with a
326 mean value of 10.5 and 55.9 kg N mon^{-1}, respectively. The corresponding simulated
327 particulate and total N losses resulted in ranges of 0.5 to 50.4 kg N mon^{-1} and 18.8 to 196.0 kg
328 N mon^{-1} with averages of 12.0 and 65.1 kg N mon^{-1}, respectively. The upgraded model
329 provided an overestimation of the particulate N loss in August 2007 and September 2008 by
330 11.3 and 14.8 kg N mon^{-1}, respectively. The particulate N losses in February 2007, March 2007,
331 July 2007 and July 2008 and total N loss in summer were underestimated. However, in terms
332 of the validation, statistical comparisons between the simulated particulate and total N losses
333 yielded significant ZIRs with R^2 values of 0.85 and 0.86 and slope values of 0.80 and 0.96,
334 nRMSE values of 57.75% and 42.55%, and NSI values of 0.74 and 0.86, respectively (n = 12;
335 Table 1). Meanwhile, the upgraded CNMM-DNDC model successfully predicted the temporal
336 variation and magnitudes of NO_3^- loss at the catchment outlet, although the model slightly
337 underestimated the peak loss in July and August of 2007 and in September of 2008 (Fig. S2).
338 As the above results demonstrated, the simulated and observed particulate and total N losses at
339 the catchment outlet indicated good agreement despite the slight underestimation of the
340 individual large values when heavy precipitation occurred.

https://doi.org/10.5194/bg-2022-238
Preprint. Discussion started: 13 February 2023

341 **3.3 Components of the simulated TN and PN at the catchment outlet**

342 The monthly components of TN and/or PN simulated from the original and upgraded
343 CNMM-DNDC model during the model validation of 2008 at the catchment outlet were
344 illustrated in Fig. 4. Among the TN components including PN, NH_4^+, dissolved organic
345 nitrogen (DON) and NO_3^-, the simulation from both of the original and upgraded
346 CNMM-DNDC demonstrated that the proportion of NO_3^- at the catchment outlet was larger
347 than that of NH_4^+ during the period from May to September when the larger precipitations
348 appeared. Moreover, the upgraded CNMM-DNDC demonstrated that the PN accounted for up
349 to 16.2%−26.6% of the TN components during the period with larger precipitations.
350 Meanwhile, the humads N accounted for 11.3%−20.3% of the PN components, though the
351 humus N accounted for the largest of the PN components. In addition, compared with the
352 original model, the upgraded model simulated the observed TN with smaller nRMSE (42.55%
353 versus 51.67%), better NSI (0.86 versus 0.80) and improved r^2 of the ZIRs (0.98 versus 0.90)
354 though no significant difference was found of the ZIRs between the original and upgraded
355 model (Fig. 4).

356 **3.4 Spatial distributions of sediment yield and particulate C, N, and P losses**

357 Figure 5 illustrated the simulated spatial distributions of the sediment yield and particulate
358 C, N, and P losses and the effects of different land uses on those in the validation year 2008.
359 The annual accumulated sediment yield simulated by the upgraded model amounted to 0−106.6
360 t ha^{-1} yr^{-1} with an average of 5.0 t ha^{-1} yr^{-1} in 2008, which was a moderate rainfall year (952
361 mm) with eight large rainstorm events (exceeding 50 mm rainfall within 24 hours). The
362 simulated annual accumulated particulate C, N, and P losses yielded 0−595.7 kg C ha^{-1} yr^{-1},

https://doi.org/10.5194/bg-2022-238
Preprint. Discussion started: 13 February 2023

0−56.0 kg N ha^{-1} yr^{-1}, and 0−7.9 kg P ha^{-1} yr^{-1} with averages of 63.6 kg C ha^{-1} yr^{-1}, 6.1 kg N ha^{-1} yr^{-1} and 0.9 kg P ha^{-1} yr^{-1}, respectively. The sloping cultivated cropland areas contributed to the greatest losses of sediment and particulate C, N, and P nutrients, with 68%, 60%, 58% and 57% of the total, respectively. Approximately 21% of sediment loss came from the residential areas as the second largest contributor to sediment loss, while the forest areas were the secondary sources to particulate C, N, and P losses, with 30%, 32%, and 32% of total losses, respectively. Meanwhile, the highest rates of the particulate C, N, and P losses per unit area occurred in the sloping cultivated cropland areas, with 84.1 kg C ha^{-1} yr^{-1}, 7.7 kg N ha^{-1} yr^{-1} and 1.1 kg P ha^{-1} yr^{-1}, respectively. However, the residential areas yielded to the highest rates of sediment, i.e., 8.6 t ha^{-1} yr^{-1}. The second largest loss rates per unit area of the particulate C, N, and P appeared in the residential areas. These results demonstrated that sediment yield and particulate C, N, and P losses caused by surface runoff in the Jieliu catchment were directly relevant to the type of land use, and the sloping cultivated cropland area became the primary source of sediment yield and particulate C, N, and P losses. Meanwhile, sediment and particulate C, N, and P losses from the residential areas could not be neglected.

Moreover, the upgraded CNMM-DNDC model coupled the biogeochemical processes with soil erosion, which was able to predict the crucial variables relevant to biogeochemical processes, including the productivity, greenhouse gases, contaminated gases and NO_3^- loss and the variables related to soil erosion, including the losses of sediment and particulate C, N and P (Fig. S3, Text S1).

https://doi.org/10.5194/bg-2022-238
Preprint. Discussion started: 13 February 2023

383 **3.5 Sediment yield and particulate C, N, and P losses under different scenarios**

384 The simulated results of the single-factor change scenarios of precipitation and
385 temperature were presented in Figure 6. The sediment yield and particulate C, N, and P losses
386 (i.e., the target variables) increased with precipitation or air temperature which was reflected by
387 the positive values. The more positive the slope value is, the greater the target variables
388 increase and vice versa. The slopes between the air temperature changes of the higher and
389 lower cooling and warming scenarios and the sediment yield changes yielded −1.25, −1.00,
390 −0.38 and −0.40, respectively. Compared to the slopes of the lower warming scenarios and the
391 lower cooling scenarios, the slopes of the higher warming scenarios and the higher cooling
392 scenarios provided 21% and 5% higher yields of sediment, respectively. Meanwhile, the
393 changes in particulate C, N, and P losses provided similar but stronger responses to the higher
394 cooling scenarios. However, the particulate nutrient losses showed a complicated response to
395 the warming scenarios. For the lower warming scenarios, the particulate nutrient losses
396 increased with air temperature. The changes in the particulate nutrient losses provided an
397 increasing tendency in response to the increase in air temperature. In terms of the higher
398 warming scenarios, the particulate nutrient losses were still increasing, but the rates of increase
399 rate decreased. These results proved that the increase in air temperature decreased the losses of
400 sediment but increased the particulate C, N, and P losses, although the promoting effect
401 became weaker for the higher warming scenarios.

402 The slopes between the precipitation changes of the higher and lower rain-reduced and
403 rain-enhanced scenarios and the sediment yield changes resulted in the values of 0.27, 0.37,

https://doi.org/10.5194/bg-2022-238
Preprint. Discussion started: 13 February 2023

404 0.52 and 0.65, respectively. In comparison with the lower rain-enhanced and rain-reduced
405 scenarios, the slopes of the higher rain-enhanced and rain-reduced scenarios provided 24%
406 higher and 34% lower yields of sediment, respectively. Meanwhile, the changes in particulate
407 nutrient losses provided similar but weaker responses to the changes in precipitation. The
408 above results demonstrated that the losses of sediment and particulate nutrients increased with
409 the increasing precipitation. In addition, the contribution from such an elevation role of
410 precipitation tended to be stronger for the higher rain-enhanced scenarios. Furthermore, the
411 changes in sediment and particulate C, N, and P losses were more sensitive to precipitation
412 scenarios than to temperature scenarios.

413 Table 2 illustrated the results of the multifactor change scenarios and the land use change
414 single-factor scenario (FL scenario). Compared to the baseline scenario, the FL scenario
415 reduced stream flow, sediment yield, and particulate nutrient losses by −12.2%, −3.6%, −5.6%,
416 −7.0%, and −7.2%, respectively. In comparison with the baseline scenario, the low GHG
417 emissions scenario with air temperature increasing by 1.5 ℃ and precipitation increasing by 10%
418 increased the stream flow, sediment yield and particulate C, N, and P losses by 21.2%, 4.1%,
419 5.3%, 5.3% and 5.3%, respectively. The increasing effects of the high GHG emissions
420 scenarios on the sediment and particulate nutrient losses were more than three times those of
421 the low GHG emissions scenarios. The low GHG emissions under the FL scenario increased
422 the stream flow and sediment yield by 5.2% and 0.2%, respectively, but decreased the
423 particulate C, N, and P losses by −0.8%, −2.3%, and −2.5%, respectively. Moreover, the high
424 GHG emissions under the FL scenario increased the stream flow, sediment yield, and

https://doi.org/10.5194/bg-2022-238
Preprint. Discussion started: 13 February 2023

425 particulate C, N, and P losses by 47.9%, 9.2%, 9.3%, 7.8%, and 7.7%, respectively. The
426 short-term and long-term no-tillage scenarios decreased the losses of particulate nutrients by
427 approximately 1% and 20%, respectively, but provided no effect on sediment yield compared
428 with the baseline scenario (data not shown).

429 **3.6 Relationship among the variables relevant to soil erosion, productivity and C/N losses**

430 Figure 7 illustrated the relationships between the variables relevant to soil erosion and
431 biogeochemistry for different land use types. No soil erosion in the RF crop system because of
432 the year-round flooding regime. For the other three land use types, the significant positive
433 correlations (r > 0.88) between sediment yield and particulate nutrients were found, because
434 they were entrained by water and moved with water flow. With regard to the SU crop system,
435 the particulate nutrients were significantly correlated with NO_3^- losses through leaching (r >
436 0.6), though the correlation coefficient between sediment yields and NO_3^- losses through
437 leaching only yielded to 0.26 (insignificantly). For the SP crop system, the variables related to
438 soil erosion (including sediment yields and particulate nutrients) were negatively correlated
439 with NH_3 emissions (r > 0.65), while they were positively correlated with NO_3^- losses through
440 runoff (r < −0.61). As to FL, significantly positive correlations between the variables related to
441 soil erosion and NO_3^- losses through leaching/runoff were found (r > 0.72).

442 ## 4. Discussion

443 **4.1 Effect of land use on soil erosion and particulate C, N, and P losses**

444 Land use change has been considered one of the most important factors affecting the
445 intensity and distribution of surface runoff and soil erosion (Dunjó et al., 2004; Kosmas et al.,
446 1997; Wei et al., 2007; Zhang et al., 2021b). Our study also provided consistent results, which

https://doi.org/10.5194/bg-2022-238
Preprint. Discussion started: 13 February 2023

447 indicated that the intensity of soil erosion and the corresponding particulate C, N, and P losses
448 in the Jieliu catchment were closely related to land use, with the following order: sloping
449 cultivated cropland > residential area > forest land. There were three major reasons why forest
450 land contributed to the lowest losses of sediment and particulate nutrients among the above
451 three land uses. First, canopy interception reduced the amount of rainfall reaching the ground,
452 which directly decreased the occurrence of runoff and subsequent erosion (Greene and Hairsine,
453 2004; Hou et al., 2020; Vasquez-Mendez et al., 2010). Several previous studies also reported
454 that forest land with a thick canopy exhibited a lower amount of runoff than did other land uses
455 (Mehri et al., 2018; Mohammad and Adam, 2010; Nunes et al., 2011). Fortunately, the direct
456 protection mechanism by canopy interception was involved in the CNMM-DNDC model,
457 which was calculated using the leaf area index (Zhang et al., 2018). Second, the litter cover of
458 forest land protects the soil surface from the direct splash and detachment of raindrops, which
459 can decrease the formation of mechanical crusts and increase the infiltration capacity and
460 hence diminish the potential for surface runoff and soil erosion (Casermeiro et al., 2004;
461 Lemenih et al., 2005; Wainwright et al., 2002). However, the CNMM-DNDC did not take the
462 protection of litter cover on the soil surface into consideration. Further observation data and
463 studies are needed to introduce the mechanism of the effect of litter cover on surface runoff and
464 soil sediment into the CNMM-DNDC model. Last, forest land is equipped with higher soil
465 organic matter and hydraulic conductivity than other land uses, which can indirectly enhance
466 soil infiltration and reduce surface runoff (Abrishamkesh et al., 2011; Fu et al., 2000; Lemenih
467 et al., 2004). The excellent soil properties of forest land soil (e.g., higher soil organic matter

https://doi.org/10.5194/bg-2022-238
Preprint. Discussion started: 13 February 2023

and vertical saturated hydraulic conductivity) have been involved in the CNMM-DNDC model inputs. Moreover, as the forest litterfall returned to the soil and participated in further C and N cycling, the content of soil organic matter was enhanced and accumulated. With regard to the scenario analysis, we found that the scenarios related to FL contributed to greater decreases in sediment yield than surface runoff (Table 2). The results of the lysimetric plot experiments by Chen et al. (2012) also demonstrated that vegetation types and human interference had a relatively small impact on surface runoff but had an appreciable effect on sediment yield.

The canopy of the cultivated cropland served as a weaker hindrance to rainfall than that of the forest canopy, which suffered from more surface runoff. Furthermore, frequent agricultural activities (i.e., tillage) loosen the subsurface soil and nutrients, which raises the risk of soil erosion and the subsequent loss of particulate nutrients (Gregorich et al., 1998; Moldenhauer et al., 1967; Muukkonen et al., 2009). The CNMM-DNDC model has taken the vertical mixing effect of tillage on the upper and lower soils into consideration, and this process left the subsurface soil organic nutrients unprotected and prone to erosion. This explained the reduction in particulate C, N, and P nutrient losses under the no-tillage scenarios (data not shown). However, several studies found that tillage disturbed the soil structure and pore size distribution (Carof et al., 2007; Castellini and Ventrella, 2012; Kay and VandenBygaart, 2002; Nunes et al., 2010), which made the effect of agricultural activities on surface runoff and soil erosion difficult to model (Leitinger et al., 2010). Given that the effect of tillage on soil was not considered in the CNMM-DNDC, the yields of surface runoff and sediment resulting from the no-tillage scenario were not decreased compared with the baseline scenario with tillage.

https://doi.org/10.5194/bg-2022-238
Preprint. Discussion started: 13 February 2023

4.2 Effect of climate change on soil erosion and particulate C, N, and P losses

In past decades, the frequent occurrence of warming and extreme weather events (e.g., extreme precipitation events) has been irrefutable (IPCC, 2019). From 1998 to 2021, the observed annual average air temperature and annual precipitation in the Jieliu catchment also presented an increasing trend but did not have a significant regression relationship (Fig. S4). The reason of why the simulated soil erosion responded to the air temperature changes might be that the climate-sensitive vegetation growth affected the C_v which was the effect factor of the soil erosion in Eq. 1. The asymmetric response of sediment yield and particulate nutrient losses to the cooling and warming scenarios might result from the different response of the vegetation growth to the cooling and warming of air temperature. Our results of the scenario analysis indicated that the losses of sediment slightly decreased with the scenarios treated with climate warming alone, which lay in the higher C_v caused by the enhanced vegetation growth (Ficklin et al., 2009; Zhang et al., 2020a; Zhou et al., 2003). We found that the decreasing effect of increasing air temperature on sediment loss decreased (especially for the scenario with an air temperature increase of 4 ℃, Fig. 6), which might be because the enhanced effect of increasing air temperature on vegetation growth is not unlimited. Once the air temperature exceeds the threshold of the optimum temperature for photosynthesis and vegetation growth, it would have a negative or even harmful impact on plant growth (Chapin, 1983; Schlenker and Roberts, 2009). The complex response of the particulate C, N, and P losses to air temperature increased, probably because they increased with ER and sediment yield, but the ER decreased with sediment. Therefore, the slightly increasing sediment with increasing air temperature and

https://doi.org/10.5194/bg-2022-238
Preprint. Discussion started: 13 February 2023

510 the corresponding decreasing ER might lead to upward or downward fluctuations in particulate
511 C, N, and P losses. However, we found that the rate of soil loss increased with increasing
512 precipitation amount and the corresponding increase in heavy rain events. Jiang et al. (2017)
513 also found that the increase in sediment loss was amplified by the increased precipitation,
514 which was directly accompanied by a dramatic and sustained increase in surface runoff.
515 Therefore, the higher GHG emissions scenarios, in which the soil erosion provided a higher
516 increase response to the rising precipitation and a lower and smaller decrease response to the
517 rising air temperature, might provide a greater risk of soil erosion than the low GHG emissions
518 scenario. Overall, our results indicated that the hydrology of the Jieliu catchment is very
519 sensitive to potential future climate changes, especially to the higher GHG emissions scenarios.

520 **4.3 Interactive effect of climate and land use change on soil and nutrient losses**

521 Changes in either climate or land use imply considerable influences on water and nutrient
522 cycles in a catchment or region (Labat et al., 2004; Milliman et al., 2008; Piao et al., 2007; Yin
523 et al., 2017). Our simulated results indicated that the reduction extent of the scenario with FL
524 on soil erosion, especially on sediment yield and subsequent nutrient losses, offset the
525 increasing extent caused by the low GHG emissions scenario. However, the scenario with FL
526 was insufficient to totally offset the sediment and particulate C, N, and P losses caused by the
527 high GHG emissions scenario. Nevertheless, vegetation restoration might still be able to slow
528 the soaring process of soil erosion caused by climate change in the future. Previous studies
529 primarily focused on the effects of human activity and climate change on the changes in
530 surface runoff or stream flow. Wang et al. (2016) demonstrated that human activity contributed

https://doi.org/10.5194/bg-2022-238
Preprint. Discussion started: 13 February 2023

to slightly larger effects on stream flow changes than climate (59% versus 41%) by analyzing the long-term records of hydrological data in the Luan River basin in North China. The results in the Heihe River basin in Northwest China showed that human activities were the dominant contributor to the variation in runoff in the upper and middle reaches when compared to climate change (Qiu et al., 2015). However, other studies have shown that the influence of climate change on soil and water loss was greater than that of human activities. Jiang et al. (2017) pointed out that climate change, in comparison with anthropogenic activities, was the primary factor causing the changes in either stream flow or sediment discharge in the Yellow River basin and Yangtze River basin in China. The Huron River catchment in southeastern Michigan in the U.S.A. was more sensitive to climate change than to land use change, as demonstrated by Barlage et al. (2002).

Furthermore, we found that the promoting impacts of both high and low GHG emissions scenarios on surface runoff were greater than those on sediment yield and subsequent particulate nutrient losses. In contrast, the reduction effect of the scenarios with FL on sediment yield and subsequent particulate nutrient losses was stronger than that on surface runoff (Table 2). These results demonstrated that human activity, e.g., the conversion from cropland with intensive human disturbance to forest land, resulted in a greater mitigation effect on sediment yield and subsequent particulate nutrient losses than on surface runoff. Therefore, further studies should consider the effects of human activity and climate change on surface runoff and on soil erosion as well as the subsequent nutrient losses. In summary, reasonable human intervention, such as rational land use change, is expected to be a feasible practice to decelerate

https://doi.org/10.5194/bg-2022-238
Preprint. Discussion started: 13 February 2023

soil erosion and subsequent particulate nutrient losses without altering and disturbing the hydrological cycle of a catchment in the context of global warming.

Conclusions

The hydro-biogeochemical model (CNMM-DNDC) was improved by introducing the soil erosion physical model (adopted from the simplified ROSE model) and the element (i.e., carbon, nitrogen and phosphorus) enrichment module to estimate soil erosion and the movements of particulate nutrients. The comparability between the simulation and observation, including surface runoff, sediment yield, and particulate nitrogen and phosphorus losses at the lysimetric plot and the stream flow, sediment yield, and particulate N loss at the outlet of Jieliu catchment, demonstrated that the upgraded CNMM-DNDC model could reliably simulate soil erosion and the consequential particulate nutrient losses. The spatial distribution characteristics of sediment yield and the consequential particulate carbon, nitrogen and phosphorus losses were directly related to the spatial distribution of land use type, among which the sloping cultivated cropland areas contributed to the greatest losses. The analysis of climate single-factor change scenarios implied that the high GHG emissions scenarios provided a greater potential risk of soil erosion, which resulted in the larger soil erosion rates than those in the low GHG emissions scenarios. The scenarios with all non-forest land changes into forest land decreased stream flow, sediment yield and particulate C, N, and P losses compared to the baseline scenario. Anthropogenic activities (e.g., land use change) might be expected to help mitigate the processes of soil and water losses accelerated by climate change in the future.

Code and data availability

The CNMM-DNDC model was originally developed by the Institute of Atmospheric

https://doi.org/10.5194/bg-2022-238
Preprint. Discussion started: 13 February 2023

574 Physics using C++ language, which can be run on a standard PC. The upgraded model is
575 available on the FigShare (https://doi.org/10.6084/m9.figshare.20210546).

576 ## Author contribution

577 Siqi Li arranged data, improved model and implemented the simulation, prepared the
578 original draft. Yong Li, Xunhua Zheng, Wei Zhang developed the conceptualization and
579 methodology of this study. Bo Zhu, Pengcheng Hu, Jihui Fan, Tao Wang collected and arranged
580 data. Shenghui Han, Rui Wang, Kai Wang analyzed data and verified the results. Zhisheng Yao,
581 Chunyan Liu improved the conceptualization and writing.

582 ## Acknowledgments

583 This work was supported by the Chinese Academy of Sciences (grant number:
584 ZDBS-LY-DQC007; XDA23070100), the special fund of State Environmental Protection Key
585 Laboratory of Formation and Prevention of Urban Air Pollution Complex
586 (SEPAir-2022080590), the National Key Scientific and Technological Infrastructure project
587 “Earth System Science Numerical Simulator Facility” (EarthLab), the National Natural Science
588 Foundation of China (grant number: 41907280, U22A20562), and the China Postdoctoral
589 Science Foundation (grant number: 2019M650808).

590 ## Competing interests

591 The authors declare that they have no conflict of interest.

592 ## References

593 Abdalla, M., Song, X., Ju, X., Topp, C., and Smith, P.: Calibration and validation of the
594 DNDC model to estimate nitrous oxide emissions and crop productivity for a summer
595 maize-winter wheat double cropping system in Hebei, China, Environmental Pollution, 262,

https://doi.org/10.5194/bg-2022-238
Preprint. Discussion started: 13 February 2023

596 114199, https://doi.org/10.1016/j.envpol.2020.114199, 2020.

597 Abrishamkesh, S., Gorji, M., and Asadi, H.: Long-term effects of land use on soil
598 aggregate stability, International Agrophysics, 25, 103–108,
599 http://www.international-agrophysics.org/Long-term-effects-of-land-use-on-soil-aggregate-stab
600 ility,106297,0,2.html, 2011.

601 Arnold, J., Srinivasan, R., Muttiah, R., and Williams, J.: Large area hydrologic modeling
602 and assessment part I: model development, Journal of the American Water Resources
603 Association, 34, 73–89, https://doi.org/10.1111/j.1752-1688.1998.tb05961.x, 1998.

604 Barlage, M., Richards, P., Sousounis, P., and Brenner, A.: Impacts of climate change and
605 land use change on runoff from a Great Lakes watershed, Journal of Great Lakes Research, 28,
606 568–582, https://doi.org/10.1016/S0380-1330(02)70606-0, 2002.

607 Berhe, A., Barnes, R., Six, J., and Mar ń-Spiotta, E.: Role of Soil Erosion in
608 Biogeochemical Cycling of Essential Elements: Carbon, Nitrogen, and Phosphorus, Annual
609 Review of Earth and Planetary Sciences, 46, 521–548,
610 https://doi.org/10.1146/annurev-earth-082517-010018, 2018.

611 Carof, M., De Tourdonnet, S., Coquet, Y., Hallaire, V., and Roger-Estrade, J.: Hydraulic
612 conductivity and porosity under conventional and no-tillage and the effect of three species of
613 cover crop in northern France, Soil Use and Management, 23, 230–237,
614 https://doi.org/10.1111/j.1475-2743.2007.00085.x, 2007.

615 Casermeiro, M., Molina, J., Caravaca, M., Costa, J., Massanet, M., and Moreno, P.:
616 Influence of scrubs on runoff and sediment loss in soils of Mediterranean climate, Catena, 57,

https://doi.org/10.5194/bg-2022-238
Preprint. Discussion started: 13 February 2023

617 91–107, https://doi.org/10.1016/s0341-8162(03)00160-7, 2004.

618 Castellini, M. and Ventrella, D.: Impact of conventional and minimum tillage on soil
619 hydraulic conductivity in typical cropping system in Southern Italy, Soil and Tillage Research,
620 124, 47–56, https://doi.org/10.1016/j.still.2012.04.008, 2012.

621 Chapin, F.: Direct and indirect effects of temperature on arctic plants, Polar Biology, 2,
622 47–52, https://doi.org/10.1007/BF00258285, 1983.

623 Chen, H., Yang, J., Fu, W., He, F., and Wang, K.: Characteristics of slope runoff and
624 sediment yield on karst hill-slope with different land-use types in northwest Guangxi,
625 Transactions of the Chinese Society of Agricultural Engineering, 28, 121–126,
626 https://doi.org/10.3969/j.issn.1002-6819.2012.16.019, 2012.

627 Cui, F., Zheng, X., Liu, C., Wang, K., Zhou, Z., and Deng, J.: Assessing biogeochemical
628 effects and best management practice for a wheat-maize cropping system using the DNDC
629 model, Biogeosciences, 11, 91−107, https://doi.org/10.5194/bg-11-91-2014, 2014.

630 Deng, J., Zhou, Z., Zhu, B., Zheng, X., Li, C., Wang, X., and Jian, Z.: Modeling nitrogen
631 loading in a small watershed in southwest China using a DNDC model with hydrological
632 enhancements, Biogeosciences, 8, 2999–3009, https://doi.org/10.5194/bg-8-2999-2011, 2011.

633 Dey, P. and Mishra, A.: Separating the impacts of climate change and human activities on
634 streamflow: a review of methodologies and critical assumptions, Journal of Hydrology, 548,
635 278–290, https://doi.org/10.1016/j.jhydrol.2017.03.014, 2017.

636 Donovan, M.: Modelling soil loss from surface erosion at high-resolution to better
637 understand sources and drivers across land uses and catchments; a national-scale assessment of

https://doi.org/10.5194/bg-2022-238
Preprint. Discussion started: 13 February 2023

638 Aotearoa, New Zealand, Environmental Modelling & Software, 147, 105228,
639 https://doi.org/10.1016/j.envsoft.2021.105228, 2022.

640 Dubache, G., Li, S., Zheng, X., Zhang, W., and Deng, J.: Modeling ammonia
641 volatilization following urea application to winter cereal fields in the United Kingdom by a
642 revised biogeochemical model, Science of The Total Environment, 660, 1403–1418,
643 https://doi.org/10.1016/j.scitotenv.2018.12.407, 2019.

644 Dunjó, G., Pardini, G., and Gispert, M.: The role of land use–land cover on runoff
645 generation and sediment yield at a microplot scale, in a small Mediterranean catchment,
646 Journal of Arid Environments, 57, 99–116, https://doi.org/10.1016/S0140-1963(03)00097-1,
647 2004.

648 Ekholm, P. and Lehtoranta, J.: Does control of soil erosion inhibit aquatic eutrophication,
649 Journal of Environmental Management, 93, 140–146,
650 https://doi.org/10.1016/j.jenvman.2011.09.010, 2012.

651 Ferrant, S., Oehler, F., Durand, P., Ruiz, L., Salmon-Monviola, J., Justes, E., Dugast, P.,
652 Probst, A., Probst, J., and Sanchez-Perez, J.: Understanding nitrogen transfer dynamics in a
653 small agricultural catchment: comparison of a distributed (TNT2) and a semi distributed
654 (SWAT) modeling approaches, Journal of Hydrology, 406, 1–15,
655 https://doi.org/10.1016/j.jhydrol.2011.05.026, 2011.

656 Ficklin, D., Luo, Y., Luedeling, E., and Zhang, M.: Climate change sensitivity assessment
657 of a highly agricultural watershed using SWAT, Journal of Hydrology, 374, 16–29,
658 https://doi.org/10.1016/j.jhydrol.2009.05.016, 2009.

https://doi.org/10.5194/bg-2022-238
Preprint. Discussion started: 13 February 2023

659 Fu, B., Chen, L., Ma, K., Zhou, H., and Wang, J.: The relationships between land use and
660 soil conditions in the hilly area of the loess plateau in northern Shaanxi, China, Catena, 39,
661 69–78, https://doi.org/10.1016/s0341-8162(99)00084-3, 2000.
662 Garcia-Ruiz, J., Begueria, S., Nadal-Romero, E., Gonzalez-Hidalgo, J., Lana-Renault, N.,
663 and Sanjuan, Y.: A meta-analysis of soil erosion rates across the world, Geomorphology, 239,
664 160–173, https://doi.org/10.1016/j.geomorph.2015.03.008, 2015.
665 Greene, R. and Hairsine, P.: Elementary processes of soil-water interaction and thresholds
666 in soil surface dynamics: a review, Earth Surface Processes and Landforms, 29, 1077–1091,
667 https://doi.org/10.1002/esp.1103, 2004.
668 Gregorich, E., Greer, K., Anderson, D., and Liang, B.: Carbon distribution and losses:
669 erosion and deposition effects, Soil and Tillage Research, 47, 291–302,
670 https://doi.org/10.1016/S0167-1987(98)00117-2, 1998.
671 Hou, G., Bi, H., Huo, Y., Wei, X., Zhu, Y., Wang, X., and Liao, W.: Determining the
672 optimal vegetation coverage for controlling soil erosion in Cynodon dactylon grassland in
673 North China, Journal of Cleaner Production, 244, 118771,
674 https://doi.org/10.1016/j.jclepro.2019.118771, 2020.
675 Hu, P.: Applicability of revised DNDC model to simulate phosphorus migration on the
676 slope farmland of purple soil, Institute of Mountain Hazards and Environment, University of
677 Chinese Academy of Sciences, Chengdu, 2020.
678 IPCC: Climate Change and Land: an IPCC Special Report on Climate Change,
679 Desertification, Land Degradation, Sustainable Land Management, Food Security, and

https://doi.org/10.5194/bg-2022-238
Preprint. Discussion started: 13 February 2023

680 Greenhouse Gas Fluxes in Terrestrial Ecosystems, 2019.

681 IPCC: Sixth Assessment Report: Working Group I: Summary for Policemakers, 2021.

682 Jetten, V., Govers, G., and Hessel, R.: Erosion models: quality of spatial predictions,
683 Hydrological Processes, 17, 887–900, https://doi.org/10.1002/hyp.1168, 2003.

684 Jiang, C., Zhang, L., and Tang, Z.: Multi-temporal scale changes of streamflow and
685 sediment discharge in the headwaters of Yellow River and Yangtze River on the Tibetan
686 Plateau, China, Ecological Engineering, 102, 240–254,
687 https://doi.org/10.1016/j.ecoleng.2017.01.029, 2017.

688 Kay, B. and VandenBygaart, A. : Conservation tillage and depth stratification of porosity
689 and soil organic matter, Soil and Tillage Research, 66, 107–118,
690 https://doi.org/10.1016/S0167-1987(02)00019-3, 2002.

691 Kosmas, C., Danalatos, N., Cammeraat, L., Chabart, M., Diamantopoulos, J., Farand, R.,
692 Gutierrez, L., Jacob, A., Marques, H., Martinez-Fernandez, J., Mizara, A., Moustakas, N.,
693 Nicolau, J., Oliveros, C., Pinna, G., Puddu, R., Puigdefabregas, J., Roxo, M., Simao, A.,
694 Stamou, G., Tomasi, N., Usai, D., and Vacca, A.: The effect of land use on runoff and soil
695 erosion rates under Mediterranean conditions, Catena, 29, 45−59,
696 https://doi.org/10.1016/S0341-8162(96)00062-8, 1997.

697 Labat, D., Godderis, Y., Probst, J., and Guyot, J.: Evidence for global runoff increase
698 related to climate warming, Advances in Water Resources, 27, 631–642,
699 https://doi.org/10.1016/j.advwatres.2004.02.020 ,2004.

700 Leitinger, G., Tasser, E., Newesely, C., Obojes, N., and Tappeiner, U.: Seasonal dynamics

https://doi.org/10.5194/bg-2022-238
Preprint. Discussion started: 13 February 2023

701 of surface runoff in mountain grassland ecosystems differing in land use, Journal of Hydrology,
702 385, 95–104, https://doi.org/10.1016/j.jhydrol.2010.02.006, 2010.

703 Lemenih, M., Karltun, E., and Olsson, M.: Assessing soil chemical and physical property
704 responses to deforestation and subsequent cultivation in smallholders farming system in
705 Ethiopia, Agriculture, Ecosystems & Environment, 105, 373–386,
706 https://doi.org/10.1016/j.agee.2004.01.046, 2005.

707 Lemenih, M., Olsson, M., and Karltun, E.: Comparison of soil attributes under Cupressus
708 lusitanica and Eucalyptus saligna established on abandoned farmlands with continuously
709 cropped farmlands and natural forest in Ethiopia, Forest Ecology and Management, 195, 57–67,
710 https://doi.org/10.1016/j.foreco.2004.02.055, 2004.

711 Li, C., Frolking, S., and Frolking, T.: A model of nitrous oxide evolution from soil driven
712 by rainfall events: 1. Model structure and sensitivity, Journal of Geophysical
713 Research–Atmospheres, 97, 9759–9776, https://doi.org/10.1029/92jd00509, 1992.

714 Li, S., Li, Y., Zhang, W., Zheng, X., Hu, P., Fan, J., Wang, T., and Zhu, B.: Simulation of
715 water-induced erosion and transport of particulate elements in catchment by extending the
716 CNMM-DNDC model, Chinese Journal of Eco-Agriculture,
717 https://doi.org/10.12357/cjea.20210781 2022a.

718 Li, S., Zhang, W., Zheng, X., Li, Y., Han, S., Wang, R., Wang, K., Yao, Z., Liu, C., and
719 Zhang, C.: Update a biogeochemical model with process-based algorithms to predict ammonia
720 volatilization from fertilized uplands and rice paddy fields, Biogeosciences, 2022, 3001–3019,
721 https://doi.org/10.5194/bg-19-3001-2022, 2022b.

https://doi.org/10.5194/bg-2022-238
Preprint. Discussion started: 13 February 2023

722 Li, Y., Shen, J., Wang, Y., Gao, M., Liu, F., and Zhou, P.: CNMM: a grid-based
723 spatially-distributed catchment simulation model, China Science Press, Beijing, 2017.
724 Liu, Y., Fu, B., Liu, Y., Zhao, W., and Wang, S.: Vulnerability assessment of the global
725 water erosion tendency: vegetation greening can partly offset increasing rainfall stress, Land
726 Degradation & Development, 30, 1061–1069, https://doi.org/10.1002/ldr.3293, 2019.
727 Loch, R. and Donnollan, T.: Field rainfall simulator studies on two clay soils of the
728 Darling Downs, Queensland. II. Aggregate breakdown, sediment properties and soil erodibility,
729 Australian Journal of Soil Research, 21, 47−58, https://doi.org/10.1071/sr9830047, 1983.
730 Ma, X., Zhao, C., and Zhu, J.: Aggravated risk of soil erosion with global warming: a
731 global meta-analysis, Catena, 200, 105129, https://doi.org/10.1016/j.catena.2020.105129,
732 2021.
733 Massey, H. and Jackson, M.: Selective erosion of soil fertility constituents, Soil Science
734 Society of America Proceedings, 16, 353−356,
735 https://doi.org/10.2136/sssaj1952.03615995001600040008x, 1952.
736 McElroy, A., Chiu, S., Nebgen, J., and Bennett, F.: Loading functions for assessment of
737 water pollution from nonpoint sources, Midwest Research Institute, Kansas City, 1976.
738 Mehri, A., Salmanmahiny, A., Tabrizi, A., Mirkarimi, S., and Sadoddin, A.: Investigation
739 of likely effects of land use planning on reduction of soil erosion rate in river basins: case study
740 of the Gharesoo River Basin, Catena, 167, 116–129,
741 https://doi.org/10.1016/j.catena.2018.04.026, 2018.
742 Meinen, B. and Robinson, D.: From hillslopes to watersheds: Variability in model

https://doi.org/10.5194/bg-2022-238
Preprint. Discussion started: 13 February 2023

743 outcomes with the USLE, Environmental Modelling & Software, 146, 105229,
744 https://doi.org/10.1016/j.envsoft.2021.105229, 2021.

745 Milliman, J., Farnsworth, K., Jones, P., Xu, K., and Smith, L.: Climatic and anthropogenic
746 factors affecting river discharge to the global ocean, 1951–2000, Global and Planetary Change,
747 62, 187–194, https://doi.org/10.1016/j.gloplacha.2008.03.001, 2008.

748 Mohammad, A. and Adam, M.: The impact of vegetative cover type on runoff and soil
749 erosion under different land uses, Catena, 81, 97–103,
750 https://doi.org/10.1016/j.catena.2010.01.008, 2010.

751 Moldenhauer, W., Wischmei, W., and Parker, D.: Influence of crop management on runoff
752 erosion and soil properties of a Marshall silty clay loam, Soil Science Society of America
753 Proceedings, 31, 541–546, https://doi.org/10.2136/sssaj1967.03615995003100040031x, 1967.

754 Muukkonen, P., Hartikainen, H., and Alakukku, L.: Effect of soil structure disturbance on
755 erosion and phosphorus losses from Finnish clay soil, Soil and Tillage Research, 103, 84–91,
756 https://doi.org/10.1016/j.still.2008.09.007, 2009.

757 Nunes, A., de Almeida, A., and Coelho, C.: Impacts of land use and cover type on runoff
758 and soil erosion in a marginal area of Portugal, Applied Geography, 31, 687–699,
759 https://doi.org/10.1016/j.apgeog.2010.12.006, 2011.

760 Nunes, A., Coelho, C., de Almeida, A., and Figueiredo, A.: Soil erosion and hydrological
761 response to land abandonment in a central inland area of Portugal, Land Degradation &
762 Development, 21, 260–273, https://doi.org/10.1002/ldr.973, 2010.

763 Panagos, P., Borrelli, P., and Robinson, D.: Tackling soil loss across Europe, Nature, 526,

https://doi.org/10.5194/bg-2022-238
Preprint. Discussion started: 13 February 2023

764 195, https://doi.org/10.1038/526195d, 2015.

765 Piao, S., Friedlingstein, P., Ciais, P., de Noblet-Ducoudré, N., Labat, D., and Zaehle, S.:
766 Changes in climate and land use have a larger direct impact than rising CO2 on global river
767 runoff trends, Proceedings of the National Academy of Sciences of the United States of
768 America, 104, 15242–15247, https://doi.org/10.1073/pnas.0707213104, 2007.

769 Pohlert, T., Huisman, J., Breuer, L., and Frede, H.: Integration of a detailed
770 biogeochemical model into SWAT for improved nitrogen predictions: model development,
771 sensitivity, and GLUE analysis, Ecological Modelling, 203, 215–228,
772 https://doi.org/10.1016/j.ecolmodel.2006.11.019, 2007.

773 Qiu, L., Peng, D., Xu, Z., and Liu, W.: Identification of the impacts of climate changes
774 and human activities on runoff in the upper and middle reaches of the Heihe River basin, China,
775 Journal of Water and Climate Change, 7, 251–262, https://doi.org/10.2166/wcc.2015.115,
776 2015.

777 Renard, K., Foster, G., Weesies, G., McCool, D., and Yoder, D.: Predicting soil erosion by
778 water: a guide to conservation planning with the Revised Universal Soil Loss equation
779 (RUSLE), Agricultural Handbook Service, United States Department of Agriculture,
780 Washington, 1997.

781 Rose, C., Williams, J., Sander, G., and Barry, D.: A mathematical model of soil erosion
782 and deposition processes: I. theory for a plane land element, Soil Science Society of America
783 Journal, 47, 991–995, https://doi.org/10.2136/sssaj1983.03615995004700050030x, 1983.

784 Schiettecatte, W., Gabriels, D., Cornelis, W., and Hofman, G.: Enrichment of organic

https://doi.org/10.5194/bg-2022-238
Preprint. Discussion started: 13 February 2023

785 carbon in sediment transport by interrill and rill erosion processes, Soil Science Society of
786 America Journal, 72, 50–55, https://doi.org/10.2136/sssaj2007.0201, 2008.
787 Schlenker, W. and Roberts, M.: Nonlinear temperature effects indicate severe damages to
788 US crop yields under climate change, Proceedings of the National Academy of Sciences of the
789 United States of America, 106, 15594–15598, https://doi.org/10.1073/pnas.0906865106, 2009.
790 Sharpley, A.: The enrichment of soil Phosphorus in runoff sediments, Journal of
791 Environmental Quality, 9, 521–526, https://doi.org/10.2134/jeq1980.00472425000900030039x,
792 1980.
793 Smith, P., Smith, J., Powlson, D., McGill, W., Arah, J., Chertov, O., Coleman, K., Franko,
794 U., Frolking, S., Jenkinson, D., Jensen, L., Kelly, R., Klein-Gunnewiek, H., Komarov, A., Li,
795 C., Molina, J., Mueller, T., Parton, W., Thornley, J., and Whitmore, A.: A comparison of the
796 performance of nine soil organic matter models using datasets from seven long-term
797 experiments, Geoderma, 81, 153–225, https://doi.org/10.1016/s0016-7061(97)00087-6, 1997.
798 Stewart, B.: Advance in soil science, Springer-Verlag, New York Berlin Heidelberg Tokyo,
799 18–55, 1985.
800 Sumner, H., Wauchope, R., Truman, C., Dowler, C., and Hook, J.: Rainfall simulator and
801 plot design for mesoplot runoff studies, Transactions of the ASAE, 39, 125–130,
802 https://doi.org/10.13031/2013.27489, 1996.
803 Teixeira, P. and Misra, R.: Measurement and prediction of nitrogen loss by simulated
804 erosion events on cultivated forest soils of contrasting structure, Soil and Tillage Research, 83,
805 204–217, https://doi.org/10.1016/j.still.2004.07.014, 2005.

https://doi.org/10.5194/bg-2022-238
Preprint. Discussion started: 13 February 2023

806 Vasquez-Mendez, R., Ventura-Ramos, E., Oleschko, K., Hernandez-Sandoval, L., Parrot,
807 J., and Nearing, M.: Soil erosion and runoff in different vegetation patches from semiarid
808 Central Mexico, Catena, 80, 162–169, https://doi.org/10.1016/j.catena.2009.11.003, 2010.
809 Wainwright, J., Parsons, A., Schlesinger, W., and Abrahams, A.: Hydrology–vegetation
810 interactions in areas of discontinuous flow on a semi-arid bajada, Southern New Mexico,
811 Journal of Arid Environments, 51, 319–338, https://doi.org/10.1006/jare.2002.0970, 2002.
812 Wan, Y. and El-Swaify, S.: Sediment enrichment mechanisms of organic carbon and
813 phosphorus in a well-aggregated Oxisol, Journal of Environmental Quality, 27, 132−138,
814 https://doi.org/10.2134/jeq1998.00472425002700010019x, 1998.
815 Wang, H., Chen, L., and Yu, X.: Distinguishing human and climate influences on
816 streamflow changes in Luan River basin in China, Catena, 136, 182–188,
817 https://doi.org/10.1016/j.catena.2015.02.013, 2016.
818 Wei, W., Chen, L., Fu, B., Huang, Z., Wu, D., and Gui, L.: The effect of land uses and
819 rainfall regimes on runoff and soil erosion in the semi-arid loess hilly area, China, Journal of
820 Hydrology, 335, 247–258, https://doi.org/10.1016/j.jhydrol.2006.11.016, 2007.
821 Williams, J. and Hann, R.: Optimal operation of large agricultural watersheds with water
822 quality constraints, Texas Water Resource Institute, Texas A&M University, Texas, 1978.
823 Wischmeier, W. and Smith, D.: Predicting rainfall erosion losses: a guide to conservation
824 planning, Agricultural Handbook, Science and Education Administration, United States
825 Department of Agriculture, Washington, 1978.
826 Yang, D., Kanae, S., Oki, T., Koike, T., and Musiake, K.: Global potential soil erosion

https://doi.org/10.5194/bg-2022-238
Preprint. Discussion started: 13 February 2023

827 with reference to land use and climate changes, Hydrological Processes, 17, 2913–2928,
828 https://doi.org/10.1002/hyp.1441, 2003.

829 Yin, J., He, F., Xiong, Y., and Qiu, G.: Effects of land use/land cover and climate changes
830 on surface runoff in a semi-humid and semi-arid transition zone in northwest China, Hydrology
831 and Earth System Sciences, 21, 183–196, https://doi.org/10.5194/hess-21-183-2017, 2017.

832 Zeng, S., Zhan, C., Sun, F., Du, H., and Wang, F.: Effects of climate change and human
833 activities on surface runoff in the Luan river basin, Advances in Meteorology, 6, 1–12,
834 https://doi.org/10.1155/2015/740239, 2015.

835 Zhang, F., Shi, X., Zeng, C., Wang, L., Xiao, X., Wang, G., Chen, Y., Zhang, H., Lu, X.,
836 and Immerzeel, W.: Recent stepwise sediment flux increase with climate change in the Tuotuo
837 River in the central Tibetan Plateau, Science Bulletin, 65, 410–418,
838 https://doi.org/10.1016/j.scib.2019.12.017, 2020a.

839 Zhang, W., Li, Y., Zhu, B., Zheng, X., Liu, C., Tang, J., Su, F., Zhang, C., Ju, X., and
840 Deng, J.: A process-oriented hydro-biogeochemical model enabling simulation of gaseous
841 carbon and nitrogen emissions and hydrologic nitrogen losses from a subtropical catchment,
842 Science of the Total Environment, 616, 305–317,
843 https://doi.org/10.1016/j.scitotenv.2017.09.261, 2018.

844 Zhang, W., Yao, Z., Zheng, X., Liu, C., Wang, R., Wang, K., Li, S., Han, S., Zuo, Q., and
845 Shi, J.: Effects of fertilization and stand age on N_2O and NO emissions from tea plantations: a
846 site-scale study in a subtropical region using a modified biogeochemical model, Atmospheric
847 Chemistry and Physics, 20, 6903–6919, https://doi.org/10.5194/acp-20-6903-2020, 2020.

https://doi.org/10.5194/bg-2022-238
Preprint. Discussion started: 13 February 2023

848 Zhang, W., Li, S., Han, S., Zheng, X., Xie, H., Lu, C., Sui, Y., Wang, R., Liu, C., Yao, Z.,
849 and Li, T.: Less intensive nitrate leaching from Phaeozems cultivated with maize generally
850 occurs in northeastern China, Agriculture, Ecosystems & Environment, 310, 107303,
851 https://doi.org/10.1016/j.agee.2021.107303, 2021a.
852 Zhang, X., Song, J., Wang, Y., Deng, W., and Liu, Y.: Effects of land use on slope runoff
853 and soil loss in the Loess Plateau of China: a meta-analysis, Science of The Total Environment,
854 755, 142418, https://doi.org/10.1016/j.scitotenv.2020.142418, 2021b.
855 Zhou, L., Kaufmann, R., Tian, Y., Myneni, R., and Tucker, C.: Relation between
856 interannual variations in satellite measures of northern forest greenness and climate between
857 1982 and 1999, Journal of Geophysical Research-Atmospheres, 108, ACL 3-1–ACL 3-16,
858 https://doi.org/10.1029/2002jd002510, 2003.
859 Zhu, B., Wang, T., Kuang, F., Luo, Z., Tang, J., and Xu, T.: Measurements of nitrate
860 leaching from a hillslope cropland in the Central Sichuan Basin, China, Soil Science Society of
861 America Journal, 73, 1419–1426, https://doi.org/10.2136/sssaj2008.0259, 2009.
862

https://doi.org/10.5194/bg-2022-238
Preprint. Discussion started: 13 February 2023

863 Table 1 Performance of the revised CNMM-DNDC model in simulating the stream flow,
864 sediment, and particulate and total nitrogen (N) losses at the Jieliu catchment outlet from 2007 to
865 2008. Total N refers to the total amount of NH_4^+, NO_3^-, dissolved organic N and particulate N.

Variables	Operation	Size	nRMSE	NSI	ZIR		
					Slope	R^2	p
Stream flow	Calibration	12	18.29	0.98	0.95	0.98	< 0.001
	Validation	12	34.57	0.89	0.85	0.94	< 0.001
Sediment loss	Calibration	12	34.02	0.94	0.91	0.96	< 0.001
	Validation	12	38.23	0.89	0.88	0.92	< 0.05
Particulate N loss	Calibration	12	49.45	0.87	0.93	0.88	< 0.001
	Validation	12	57.75	0.74	0.80	0.85	< 0.001
Total N loss	Calibration	12	56.98	0.86	1.21	0.90	< 0.001
	Validation	12	42.55	0.86	0.96	0.86	< 0.001

866 The statistical criteria used to quantify the discrepancy between observations and simulations
867 include the normalized root mean square error (nRMSE), the Nash–Sutcliffe index (NSI) and the
868 slope, determination coefficient (R^2) and significance level (p) of the zero-intercept univariate
869 linear regression (ZIR). Size represents the sample size.
870
871

https://doi.org/10.5194/bg-2022-238
Preprint. Discussion started: 13 February 2023

872 Table 2 Simulated comprehensive effects of precipitation, air temperature and land use change
873 on surface runoff, sediment yield, and particulate carbon (C), nitrogen (N) and phosphorus (P)
874 losses in the validation year of 2008. The low greenhouse gas (GHG) emission scenario
875 represents the scenario of air temperature increasing by 1.5 ℃ and precipitation increasing by
876 10%. The high GHG emission scenario represents the scenario of an air temperature increase of
877 4 ℃ and a precipitation increase of 30%. The FL scenario is the abbreviation of the scenario of
878 upland change into forest land.

	Change between the scenario and the baseline (%)				
Scenario	Surface runoff	Sediment yield	Particulate C	Particulate N	Particulate P
Low GHG	21.2	4.1	5.3	5.3	5.3
High GHG	72.9	14.8	17.8	18.0	18.1
FL	−12.2	−3.6	−5.6	−7.0	−7.2
Low GHG with FL	5.2	0.2	−0.8	−2.3	−2.5
High GHG with FL	47.9	9.2	9.3	7.8	7.7

879

880

https://doi.org/10.5194/bg-2022-238
Preprint. Discussion started: 13 February 2023

881

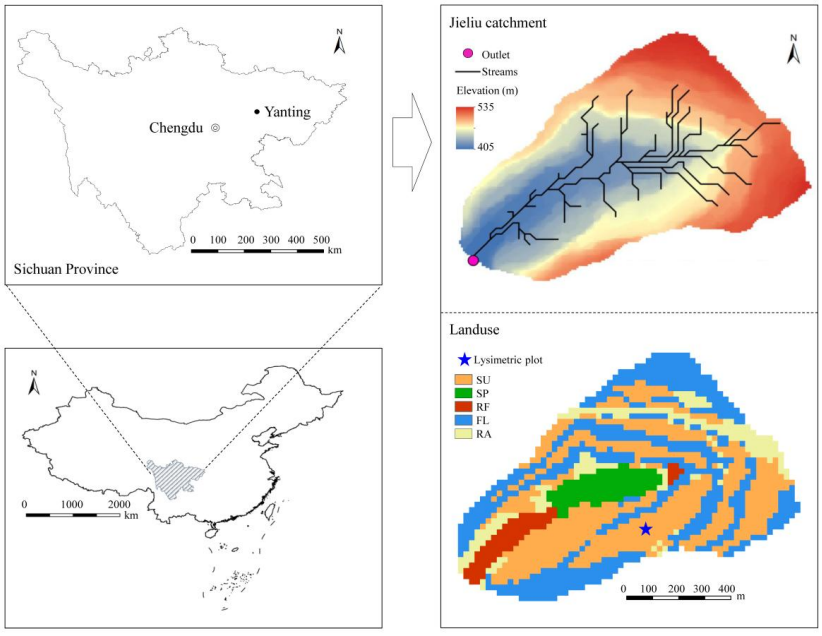

882

883 Fig. 1 The location, digital elevation model and land use types of the Jieliu catchment. The land
884 use types are the sloping uplands with the summer maize−winter wheat rotation (SU), seasonally
885 waterlogged paddy with the paddy rice−winter wheat rotation or paddy rice−rape rotation (SP),
886 the winter-flooding paddy with the paddy rice-flooding fallow regime (RF) and the forest land
887 (FL).

888

https://doi.org/10.5194/bg-2022-238
Preprint. Discussion started: 13 February 2023

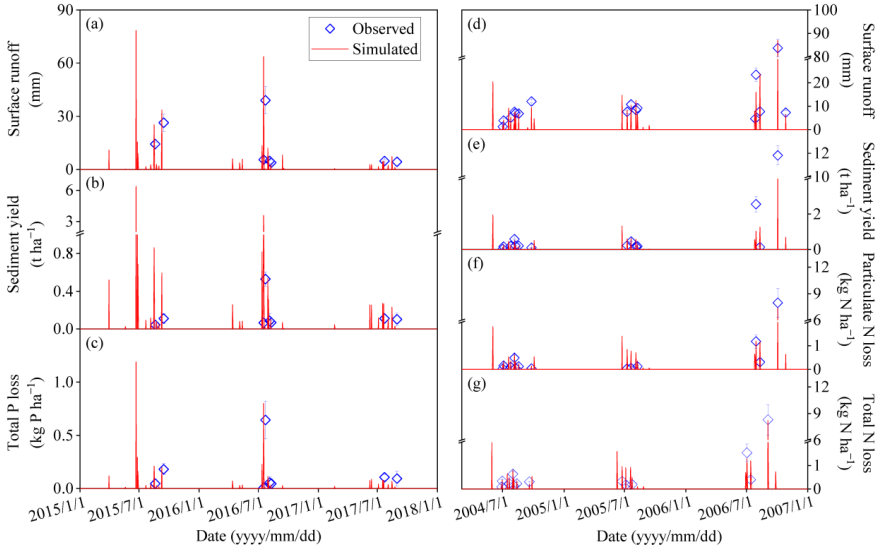

Fig. 2 Observed and simulated surface runoff (a), sediment yield (b) and total phosphorus (P) losses (c) from 2015 to 2017 and surface runoff (d), sediment yield (e), particulate nitrogen (N) loss (f) and total N loss (g) from 2015 to 2017 in the lysimetric plot. Total P refers to the dissolved and particulate P. Total N refers to the total amount of NH_4^+, NO_3^-, dissolved organic N and particulate N. The vertical bars indicate the standard error of three spatial replicates. The observed data cited from Deng et al. (2011), Zhang et al. (2018), Li et al. (2022) and Hu (2020) were provided by Bo Zhu.

https://doi.org/10.5194/bg-2022-238
Preprint. Discussion started: 13 February 2023

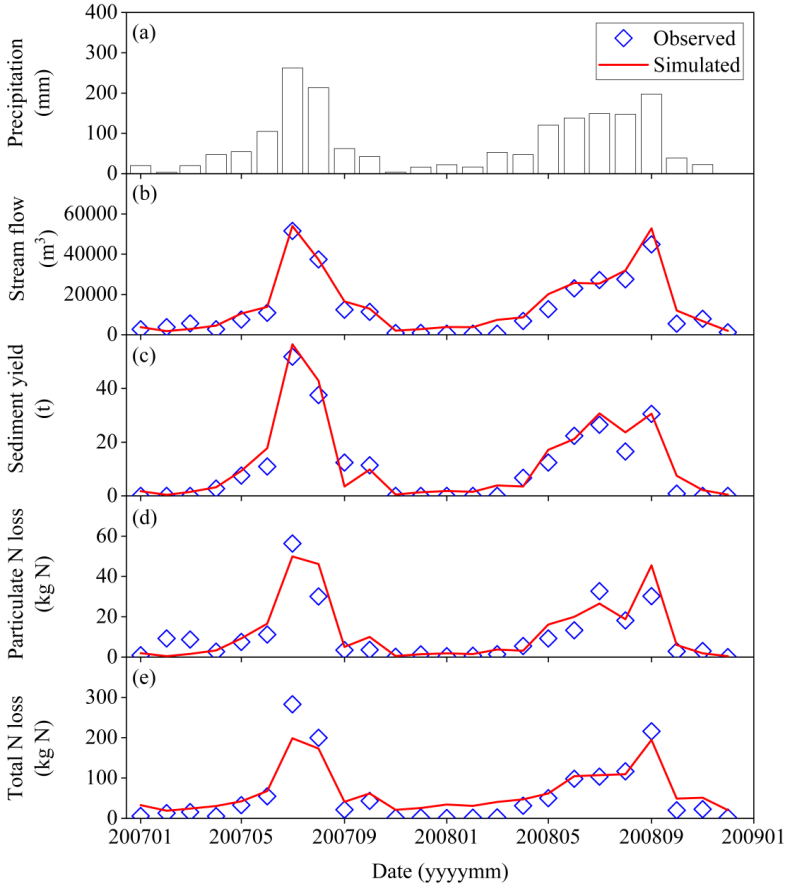

898

899 Fig. 3 Monthly observed precipitation (a), observed and simulated stream flow (b), sediment
900 yield (c), particulate nitrogen (N) loss (d) and total N loss (e) at the outlet of the Jieliu catchment
901 from 2007 to 2008. Total N refers to the total amount of NH_4^+, NO_3^-, dissolved organic N and
902 particulate N. The observed data cited from Deng et al. (2011) and Zhang et al. (2018) were
903 provided by Bo Zhu.

904

https://doi.org/10.5194/bg-2022-238
Preprint. Discussion started: 13 February 2023

Biogeosciences
Discussions
Open Access
EGU

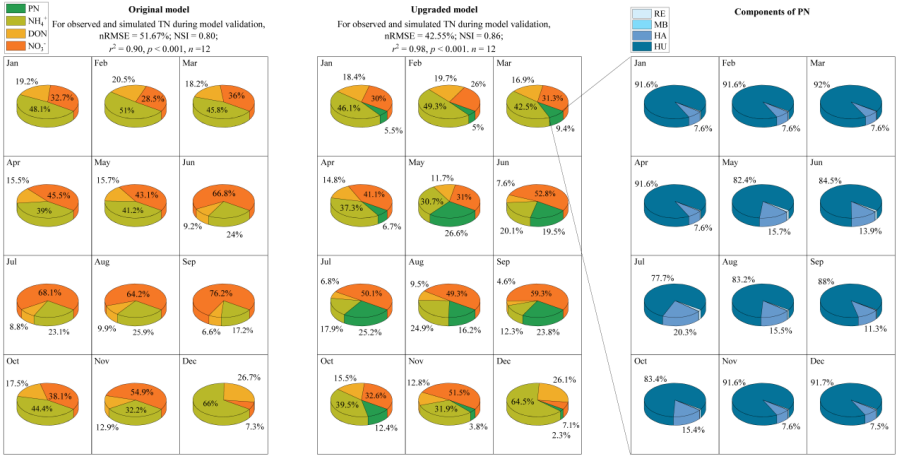

905

906 Fig. 4 Components of the simulated total nitrogen (TN) and/or particulate N (PN) of the
907 original and upgraded CNMM-DNDC model during the model validation. DON is the
908 abbreviation of the dissolved organic nitrogen. The components of PN are the N from residue
909 (RE), microbe (MB), humads (HA) and humus (HU).

910

https://doi.org/10.5194/bg-2022-238
Preprint. Discussion started: 13 February 2023

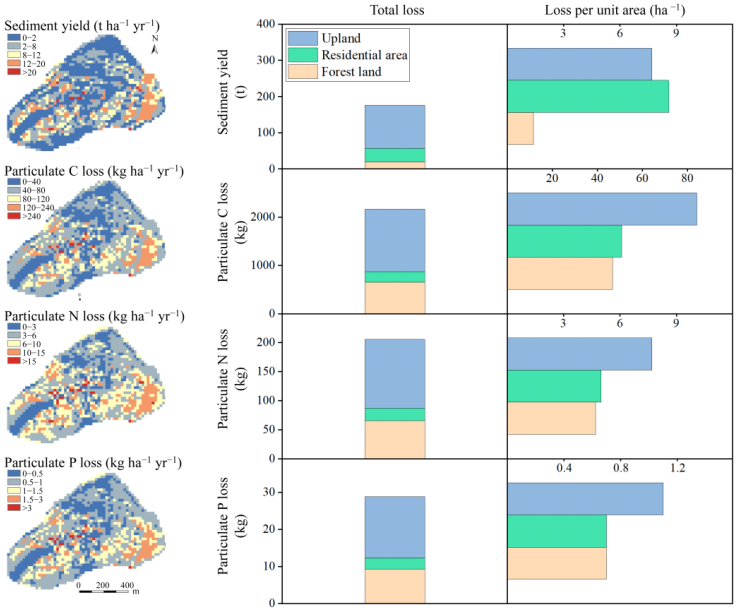

911

912 Fig. 5 Simulated spatial distributions of sediment yield, particulate carbon (C), nitrogen (N) and

913 phosphorus (P) losses and the effects of different land uses (i.e., cropland, residential area and

914 forest land) in the validation year of 2008.

915

https://doi.org/10.5194/bg-2022-238
Preprint. Discussion started: 13 February 2023

Biogeosciences Discussions Open Access EGU

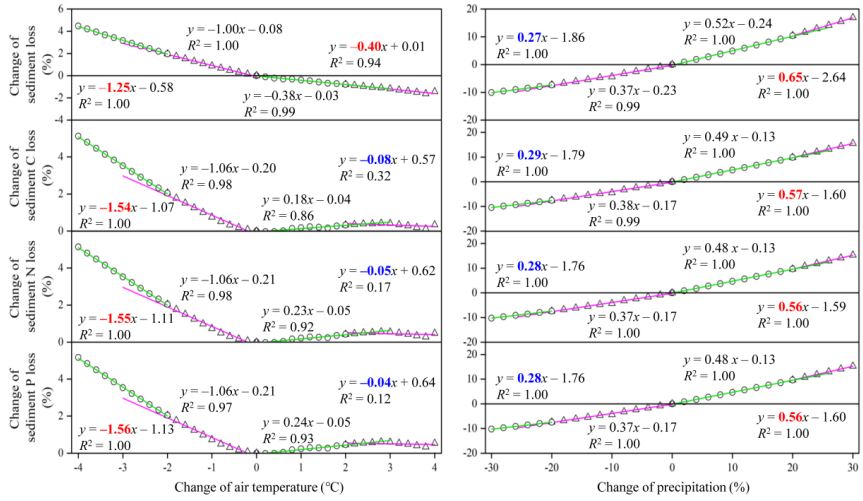

916

917 Fig. 6 Simulated effects of precipitation and air temperature change on sediment yield and
918 particulate carbon (C), nitrogen (N) and phosphorus (P) losses in the validation year of 2008.
919 The air temperature and precipitation single-factor scenarios were divided into four sets. The
920 scenarios with air temperature reductions and increases 0℃~2℃ and greater than 2℃ were
921 defined as the lower and higher cooling and warming scenarios, respectively. Similarly, the
922 scenarios with precipitation reductions and increases 0%~20% and greater than 20% were
923 defined as the lower and higher rain-reduced and rain-enhanced scenarios, respectively. The
924 numbers in blue and red in front of the letter *x* represent that the higher warming or cooling
925 scenarios (or the higher rain-enhanced or rain-reduced scenarios) result in more and lower
926 effects on sediment yield and particulate C, N and P losses than the lower ones, respectively.

927

https://doi.org/10.5194/bg-2022-238
Preprint. Discussion started: 13 February 2023

928

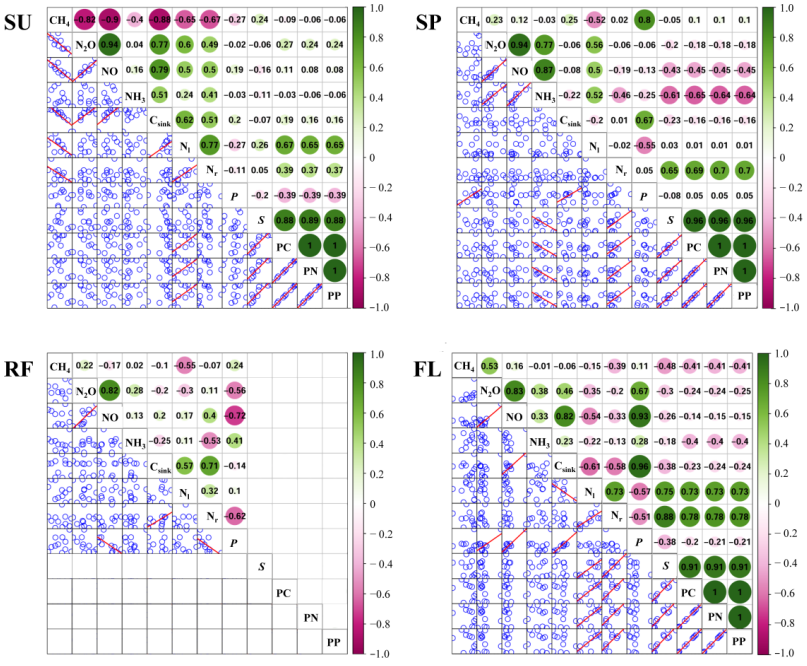

929

930 Fig. 7 Correlation analysis among the simulated sediment (S), particulate carbon (PC), nitrogen
931 (PN) and phosphorus (PP) losses, productivity (*P*), C sink density (C_{sink}), methane (CH_4), nitrous
932 oxide (N_2O), nitric oxide (NO) and ammonia (NH_3) emissions, losses of nitrate through leaching
933 (N_l) and surface runoff (N_r) for different land use types. The land use types are the sloping
934 uplands with the summer maize−winter wheat rotation (SU), seasonally waterlogged paddy with
935 the paddy rice−winter wheat rotation or paddy rice−rape rotation (SP), the winter-flooding
936 paddy with the paddy rice-flooding fallow regime (RF) and the forest land (FL). No losses of *S*,
937 PC, PN, and PP in the RF crop system because of the year-round flooding regime. The figures in
938 the circles stand for the correlation coefficients. The correlations with the level of $p < 0.05$ are
939 considered as significant and the linear regression lines are exhibited.